



High performance electrochemical capacitors from aligned carbon nanotube electrodes and ionic liquid electrolytes

Wen Lu^{a,*}, Liangti Qu^b, Kent Henry^a, Liming Dai^{b,**}

^a ADA Technologies Inc., 8100 Shaffer Parkway, Littleton, CO 80127, USA

^b Department of Chemical and Materials Engineering, University of Dayton, 300 College Park, Dayton, OH 45469, USA

ARTICLE INFO

Article history:

Received 4 December 2008

Received in revised form 8 January 2009

Accepted 8 January 2009

Available online 19 January 2009

Keywords:

Energy storage
Electrochemical capacitor
Electrode
Carbon nanotube
Electrolyte
Ionic liquid

ABSTRACT

We report a new class of electrochemical capacitors by utilizing vertically aligned carbon nanotubes as the electrodes and environmentally friendly ionic liquids (ILs) as the electrolytes. With their vertically aligned structures and well spacing, aligned carbon nanotubes showed a strong capacitive behavior in the ionic liquid electrolyte. Plasma etching played an important role in opening the end tips of nanotubes and in introducing defects and oxygenated functionalization to the nanotubes, further enhancing the capacitive behavior of carbon nanotubes. With the combined contribution from double-layer capacitance and redox pseudocapacitance, carbon nanotubes showed a remarkable capacitance in ionic liquid electrolyte. Combining the highly capacitive behavior of carbon nanotube electrodes with the large electrochemical window of ionic liquid electrolytes, the resultant capacitors showed a high cell voltage, high energy density, and high power density, potentially outperforming the current electrochemical capacitor technology. The device configuration incorporating vertically aligned nanostructured electrodes and inherently safe electrolytes would be useful for improving performances for new energy storage technologies.

© 2009 Elsevier B.V. All rights reserved.

1. Introduction

Electrochemical capacitors (aka, supercapacitors or ultracapacitors) are energy storage devices that combine the high energy storage capability of batteries with the high power delivery capability of capacitors [1,2]. Electrochemical capacitors have been developed to provide power pulses for a wide range of applications including transportation, consumer electronics, medical electronics, and military devices. However, performance (energy and power densities, safety, and cycle life) of the state-of-the-art electrochemical capacitors is needed to improve to satisfy the rapidly increasing performance demands for these applications. The maximum energy (E_{\max}) and power (P_{\max}) of an electrochemical capacitor are given by: $E_{\max} = (CU^2)/2$ (Eq. (1)) and $P_{\max} = U^2/(4R)$ (Eq. (2)), respectively (where C is capacitance, U is cell voltage, and R is total equivalent series resistance (ESR) of the capacitor) [2]. Limited properties of the presently available electrodes (low electrolyte accessibility and low capacitance) and electrolytes (narrow electrochemical window, flammability, toxicity, volatility, and thermal instability) are needed to overcome to develop high performance electrochemical capacitors with high energy and power densities, safe operation, and long lifetimes.

High-surface-area activated carbons (ACs) are currently used electrode materials in commercial electrochemical capacitors [3]. While these ACs possess a high specific surface area ($1000\text{--}2000\text{ m}^2\text{ g}^{-1}$) they have a limited capacitance. This lack of capacitance of ACs is largely associated with their low mesoporosity and low electrolyte accessibility [4]. Development of electrode materials having an appropriate balance between the surface area and the mesoporosity has been a bottleneck to the development of advanced electrochemical capacitors. Since their discovery in 1991 [5], carbon nanotubes (CNTs) have become an important class of electrode material for various electrochemical devices, including electrochemical capacitors [4,6–11]. In spite of their moderate surface area compared to ACs, CNTs show reasonably high capacitances (e.g., 102 F g^{-1} for multi-walled nanotubes [6] and 180 F g^{-1} for single-walled nanotubes [9]) due to their large mesoporosity and high electrolyte accessibility. Excellent electrical conductivity, high mesoporosity, and high electrolyte accessibility of CNTs ensure a high charge transport capability and hence a high power density for the electrochemical capacitor. Conventional aqueous [6,9,12] and organic [13–15] electrolytes have been employed for the development of CNT electrochemical capacitors. The aqueous electrolyte-based electrochemical capacitors showed reasonably high power densities ($>7\text{ kW kg}^{-1}$) but their energy densities ($\sim 4\text{ Wh kg}^{-1}$) are still limited. Narrow electrochemical window of the aqueous electrolytes used, and hence small cell voltages and low energy (as described in Eq. (1)) of the capacitors, is a major reason for this drawback. The advantage of the use of organic

* Corresponding author. Tel.: +1 303 874 8292; fax: +1 303 792 5633.

** Corresponding author. Tel.: +1 937 229 2670; fax: +1 937 229 3433.

E-mail addresses: wenl@adatech.com (W. Lu), ldai@udayton.edu (L. Dai).

electrolytes is mainly associated with their relatively large electrochemical windows. To this end, in order to further enhance the capacitor performance, especially the energy density required for advanced CNT electrochemical capacitors [7], new electrolytes having even larger electrochemical windows are needed. Further, the ideal electrolytes will also offer superior safety properties over the current technology.

Currently employed electrolytes in commercial electrochemical capacitors include aqueous and organic [16]. The narrow electrochemical windows of these electrolytes (aqueous: ~ 1.2 V, organic: 2–3 V) lead to small cell voltages and hence limited energy and power of the capacitor (Eqs. (1) and (2)). Upon charge, ions of the electrolyte are transported into the double-layers at the electrode–electrolyte interfaces, resulting in the decrease of salt concentration in the electrolyte (the so-called electrolyte depletion) and hence the limit of energy density of the capacitor [17]. Also, this electrolyte depletion increases the cell resistance and thus lowers the maximum power density achievable for the capacitor. As a result, fabricated from these electrolytes and AC electrodes, the commercially available electrochemical capacitors possess a low energy density ($4\text{--}5$ Wh kg $^{-1}$) and a low power density ($1\text{--}2$ kW kg $^{-1}$) [3]. Furthermore, some organic electrolytes suffer from serious health and safety problems as they are inherently volatile, flammable, and toxic [18], resulting in a narrow operational temperature range and potential for explosion during outlying circumstances (e.g., during car accidents). Since their first description in 1914 [19], ionic liquids (ILs) have been used in a wide range of applications [20–22]. Certain unique properties of these environmentally friendly ILs, including high ionic conductivity (up to 10^{-2} S cm $^{-1}$), large liquid phase range ($-100\text{--}400$ °C), wide electrochemical window ($4\text{--}6$ V), non-volatility, non-flammability, and non-toxicity, have made them an excellent electrolyte for various electrochemical systems [23].

Given that the performance of an electrochemical capacitor is directly proportional to the square of its cell voltage, Eqs. (1) and (2), the use of large electrochemical window ILs would significantly boost the performance for CNT electrochemical capacitors. Compared to conventional electrolytes, ILs have a unique property that they are both 100% solvents and also 100% salts. It is unnecessary to add other salts into an IL to achieve ionic conductivity. The very high ionic concentration of ILs would be able to eliminate the electrolyte depletion problem as encountered with conventional electrolytes and therefore enhance the capacitor performances. Further, the superior chemical and environmental stability of ILs ensures safe operation and long lifetimes for capacitors. Previously, electrochemical behavior of randomly entangled CNT electrodes has been studied in IL electrolytes, showing a large potential window but with a limited capacitance for the CNTs [24,25]. It is likely that a facilitated access of the IL ions could not take place within the CNTs due to the mismatch between the irregular pore structures of the randomly entangled CNTs and the relatively high viscosity of the IL electrolytes (comparing to conventional aqueous and organic electrolytes). Recent research demonstrated that vertically aligned CNTs are advantageous over their randomly entangled counterparts for electrochemical capacitor applications, especially, in improving rate capability of the capacitors [14,15,26]. Specifically, in IL electrolytes, improved rate capability has been achieved for CNTs when vertically aligned structures were employed [27]. Nevertheless, for the development of high performance electrochemical capacitors, capacitance (24 F g $^{-1}$) of these CNTs (obtained in IL electrolytes) is still limited. This, therefore, indicates a need to improve the properties of CNTs in order to match with an IL to achieve a high capacitance for the CNTs and thus a high performance for the CNT-IL electrochemical capacitors.

In this work, we investigated the electrochemical behavior of plasma-etched, vertically aligned CNTs (abbreviated as ACNTs)

in IL electrolytes. Unique properties of the ACNTs made them highly capacitive in the ILs. Moreover, combining the novel properties of ACNT electrodes with the large electrochemical window of environmentally friendly IL electrolytes, we developed a new class of electrochemical capacitors, showing high cell voltages (4 V) and superior energy and power densities (148 Wh kg $^{-1}$ and 315 kW kg $^{-1}$, based on the mass of the active electrode materials), potentially outperforming the currently available electrochemical capacitor technology.

2. Experimental

Vertically aligned CNT arrays were synthesized by vacuum chemical vapor deposition on SiO $_2$ /Si wafers that were pre-deposited with 3-nm thick Fe catalysts [28,29]. The catalyst-coated substrates were first inserted into a quartz tube furnace and remained at 450 °C in air for 10 min, followed by flowing a mixture gases of 48% Ar, 28% H $_2$, and 24% C $_2$ H $_2$ under 10–100 Torr at 750 °C for 10–20 min to grow the aligned CNTs. In order to electrically contact the CNTs in the array, a gold layer was deposited to the (upper) tips of the resultant nanotubes and the CNT array was then physically removed from the silicon wafer using a commercially available double-sided conducting tape [30]. Finally, the exposed side of the CNT array was subjected to oxygen plasma etching [29]. After the plasma etching, the amorphous carbon layer that covers the CNT film can be properly removed without damaging the CNTs. Prolonged plasma treatment (>20 min) was able to cause a controllable disintegration of the graphitic structure, leading to the opening of CNT end-tips (Fig. 1). With the underlying gold layer (as the current collector), the resultant plasma-etched ACNT electrodes can be used directly without the incorporation of an insulating polymer binder. This would be able to eliminate any electrical resistance that may be deduced from a binder commonly employed in conventional electrode materials. The length of the ACNTs was adjusted by controlling the growth time and pressure. Increasing the tube length resulted in the enhanced overall surface area and thus the improved charge capacity (F cm $^{-2}$) for the ACNT electrodes. Preliminary test indicated that similar capacitance (F g $^{-1}$) was achieved for ACNT electrodes with different nanotube lengths, indicating the high electrochemical accessibility of the ACNTs even with long nanotubes. In order to ensure a high charge capacity for the electrode, a long tube length (100–200 μ m) was selected and used throughout this study. Under the same conditions, a blank electrode assembly consisting of a gold layer and a double-sided conducting tape was fabricated at the same size (2 cm 2) as for an ACNT electrode. The amount of CNT of the ACNT electrode was measured by weighing the difference between this blank assembly and the ACNT electrode with the microbalance of a Thermogravimetric Analyzer (TGA, Q500, TA Instruments) with a weighing precision of 0.1 μ g. The CNT loading of the ACNT electrode was found to be about 0.18 mg cm $^{-2}$.

Morphology of the ACNTs was investigated by scanning electron microscopy (SEM) with a Hitachi S-4800 high-resolution scanning electron microscope and by transmission electron microscopy (TEM) with a Hitachi H-7600 transmission electron microscope. Raman spectra of the ACNTs were carried out by a Renishaw inVia Micro-Raman under a laser excitation wavelength of 514 nm. X-ray photoelectron spectroscopic (XPS) measurements of the ACNTs were made by a VG Microtech ESCA 2000 using monochromatic Mg K α radiation at a power of 300 W. As reported previously [31], due to the small amount of the ACNTs obtained, their specific surface area was not measured.

In a KEMEX GB1000 dry glove box, the ACNT-IL capacitors were fabricated by sandwiching a [EMIM][Tf $_2$ N]-soaked separator (two PTFE membranes) between two ACNT electrodes. The cell assembly with an effective size of 1×1 cm 2 for the capaci-

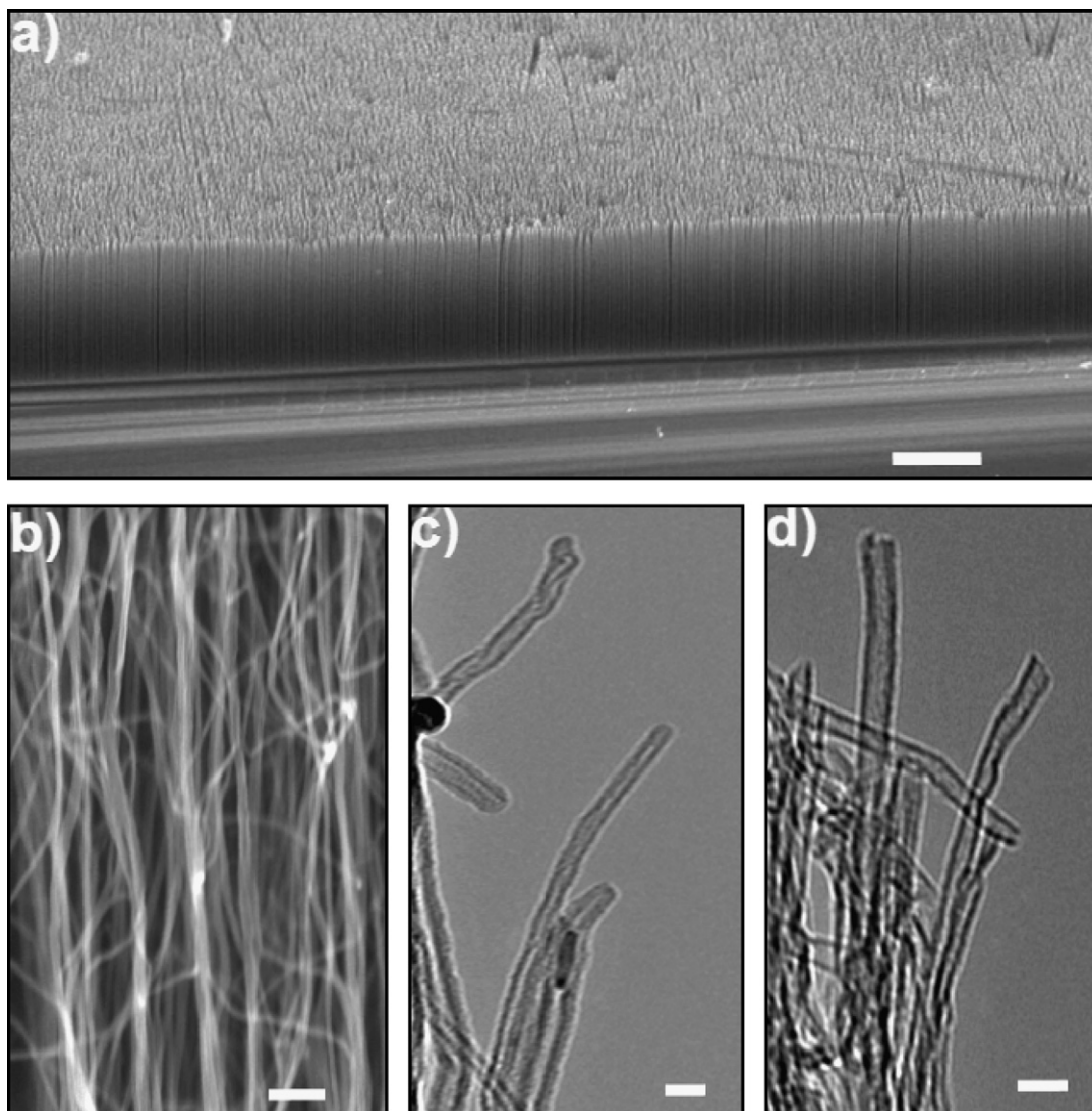


Fig. 1. (a): SEM image of a plasma-etched ACNT electrode (scale bar: 100 μm). (b): Higher magnification view of the electrode (scale bar: 100 nm). TEM images of the CNTs before (c) and after (d) plasma etching (scale bar: 20 nm). The multi-walled CNT array is highly aligned with the tube length of $\sim 150 \mu\text{m}$ and an outer and inner diameter of approximately 10 and 5 nm, respectively.

tor was then packed with two polypropylene plates and sealed with epoxy. The PTFE (poly(tetrafluoroethylene)) membrane (thickness: 23 μm , pore size: 0.05 μm , porosity: 50–70%) provided by WL Gore & Associates is highly porous and has been confirmed in our previous research [32] to be fully wettable by both hydrophobic and hydrophilic ionic liquids and thus provides a good separator material for the ionic liquid-incorporated electrochemical capacitor applications. Ionic liquid [EMIM][Tf₂N] (1-ethyl-3-methylimidazolium bis(trifluoromethylsulfonyl)imide) was purchased from Covalent Associates, Inc. In parallel, two AC electrodes (specific surface area: 1000–2000 $\text{m}^2 \text{g}^{-1}$, thickness: 150 μm , carbon loading: 9 mg cm^{-2}) were used to fabricate a reference capacitor with [EMIM][Tf₂N] (*i.e.*, the AC-IL capacitor) for evaluating the performance of the ACNT-IL capacitors.

All electrochemical measurements were performed with a PGSTAT30 potentiostat (Eco Chemie B.V.). For the testing of ACNT or AC electrodes in [EMIM][Tf₂N] (Fig. 2), a three-electrode electrochemical cell was employed, consisting of the ACNT electrode or AC electrode as the working (testing) electrode (effective size: 0.5 \times 0.5 cm^2), a platinum wire (1.5 mm diameter) as the auxiliary electrode, and a silver wire (1.5 mm diameter) as the

quasi-reference electrode. For the testing of capacitors (Fig. 6), a two-electrode system was used where the reference electrode lead and the auxiliary electrode lead were connected together as one electrode, coupling with the working electrode to make the two-electrode system. The current response in the cyclic voltammograms (CVs) was normalized with respect to the mass of the active material (ACNT or AC) of the electrodes.

3. Results and discussion

In this work, for the electrochemical study of ACNT electrodes, we employed imidazolium ILs as the electrolytes because of their relatively higher ionic conductivity and lower viscosity than other groups of ILs [33]. Specifically, among all imidazolium ILs investigated, we have determined [EMIM][Tf₂N] to be the most appropriate IL due to its superior properties of large electrochemical window (4.28 V), high ionic conductivity ($8.4 \times 10^{-3} \text{ S cm}^{-1}$), low viscosity (28 cp), high decomposition temperature (400 $^{\circ}\text{C}$), and water immiscibility. In [EMIM][Tf₂N], the ACNT electrode showed a butterfly-shape CV (Fig. 2(A)), similar to that of a randomly entangled CNT electrode [24] but with a much higher capacitance and

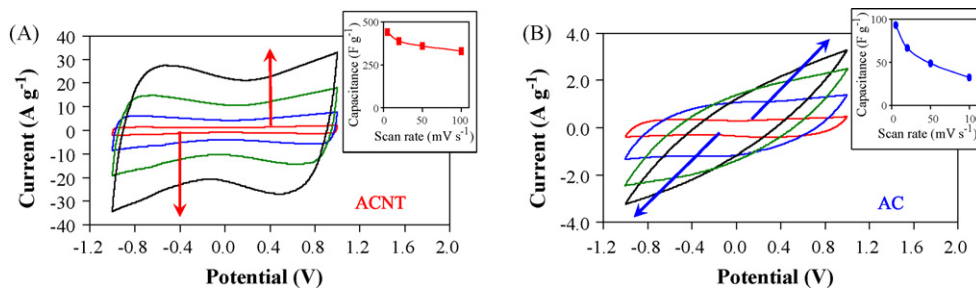


Fig. 2. CVs obtained in [EMIM][Tf₂N] for an ACNT electrode (A) and an AC electrode (B) at the scan rate increasing from 5, 20, 50, to 100 mV s⁻¹ as indicated by arrows. Insets show capacitance change of the electrodes upon the increase of scan rate.

sharper transient responses at both ends of the CV. At the scan rate of 5 mV s⁻¹, capacitance of the ACNT electrode was found to be 440 F g⁻¹ (at 1 V), which then decreased slightly upon the increase of scan rates (see the inset). This indicates the high charge storage ability and high rate capability of the ACNT electrode in the IL. Assuming a moderate specific surface area (about 400 m² g⁻¹) [34] for our multi-walled ACNTs and based on the charge storage capacity (about 50 μF cm⁻²) suggested for carbon materials [2], our ACNT electrode would produce a double-layer capacitance of about 200 F g⁻¹. Thus, the higher capacitance measured in this work for the ACNT electrode (440 F g⁻¹) would indicate some unique properties of the ACNTs. Indeed, it has been pointed out previously that the ability for charge accumulation in the electrode–electrolyte interface of CNTs strongly depends on the mesoporosity, electrolyte accessibility, diameters, and surface nature (e.g., defects and functionalization) of the CNTs [35]. Unique properties of ACNTs developed in this work are believed to be responsible for their superior capacitance in the IL.

First, mesoporosity of CNTs is essential for ion transportation in the CNTs [35]. Unlike the irregular pore structures of randomly entangled CNTs, the vertically aligned and unbundled structures and well spacing between tubes of the ACNTs (Fig. 1) provide a more mesoporous and more accessible surface [36]. This translates to a high electrolyte accessibility and a large effective surface area for the ACNTs, and thus a strong capacitive behavior for the ACNT electrode in the IL. Second, end-tip-opening of the ACNTs by plasma etching enhances the capacitive behavior of the ACNT electrode. In addition to the removal of amorphous carbons from the CNT film surface, plasma etching can also effectively open the end-tips of the nanotubes (Fig. 1(d)) [28,29]. TEM imaging (not shown) confirmed that the inner cavity of the tip-opened ACNTs can be easily filled with the IL. Similarly, accessibility of the inner cavity of tip-opened ACNTs has been demonstrated with Ag nanorod filling [29] and Li⁺ intercalation [37]. For electrochemical capacitor applications, the importance of this internal-wall-deduced access to introduce additional surface area and hence additional capacitance has been reported for tip-opened randomly entangled CNTs [35]. In the present work, with their highly aligned and unbundled structures and thus superior electrolyte accessibility over the randomly entangled CNTs, this additional capacitive contribution from the internal surfaces of the ACNTs would be more effective. According to the model proposed by Peigney et al. [34], a specific surface area of about 400 m² g⁻¹ can be estimated for our multi-walled ACNTs (with tip-opened). Therefore, with their high electrolyte accessibility discussed above, these ACNTs would produce a double-layer capacitance of about 200 F g⁻¹ [2]. Further, inner diameters of the nanotubes play an important role in determining the charge storage from the internal surfaces of nanotubes. In the case of a very large canal and only a few concentric graphitic layers which form the nanotube wall, the electrochemically active electrode–electrolyte interface of the nanotubes is very small, and thus, the canal does not play any positive role for charging the double-layer [35]. It

has been suggested that optimized CNTs for an electrochemical capacitor should possess a great number of graphene layers and an open central canal with diameter below 5 nm [35]. Indeed, this is the situation of our ACNTs that have an inner diameter of about 5 nm (Fig. 1(d)) and thus can expect a superior charge storage contribution from the internal surfaces of nanotubes. It can be expected that, as the electrolyte ions squeeze into the inner cavity of these small nanotubes, a small distance between the tube's internal surface and the maximum charge density of electrolyte ions would be deduced (comparing to that existing between the tube's external surface and the electrolyte). According to $C = \epsilon S/d$ (Eq. (3)) (where C is capacitance, ϵ is permittivity of the electrolyte, S is surface area of the electrode–electrolyte interface, d is distance between the polarized carbon surface and the maximum charge density of electrolyte ions), this small distance will make the capacitance from the internal surfaces more pronounced than that from the external surfaces of the nanotubes, resulting in an overall double-layer capacitance greater than 200 F g⁻¹ for the ACNTs. Previously, a high capacitance of 365 F g⁻¹ was reported for a template-synthesized aligned CNT electrode (with an inner diameter of 110 nm), which has been attributed to the contribution of the double-layer capacitance (from both the external and internal surfaces) and the pseudocapacitance of the nanotubes [8]. To this end, a higher capacitance would be achievable for our ACNTs due to their much smaller inner diameters (5 nm vs. 110 nm). That is, the accessibility of ILs to both the external and internal surfaces of our ACNTs provides an enhanced overall surface area and thus an improved double-layer capacitance for the ACNT electrode (as illustrated in Fig. 3), while the appropriate inner diameter of the nanotubes then enhances the capacitive contribution from the internal surfaces of the ACNTs. Third, formation of defects on the ACNTs by plasma etching further improves the capacitive behavior of the ACNT electrode. It has been pointed out that the presence of a dense pyrolytic carbon outer layer on the nanotubes is able to decrease the nanotube's electrolyte accessibility. However, destroy of this layer by defects (and thus the formation of wall roughness and the improvements in electrolyte accessibility and overall active surface area on the nanotubes) is very favorable for charging the double-layer on the CNTs [35]. As shown in Fig. 4, the pristine CNTs show a typical Raman feature with a D band (at 1330 cm⁻¹) and a G band (at 1590 cm⁻¹) [38]. The intensity ratio of the D band to the G band was about 0.5. After plasma etching, the D band became stronger, resulting in an increased D band / G band ratio of 0.96. This indicates the formation of defects along the nanotubes of the ACNTs. Broadly, structural defects of CNTs are important to facilitate the electrochemical processes occurring on the CNTs [39–43]. Therefore, this supports that, upon plasma etching, introduction of defects on the nanotubes can further improve the capacitive behavior of our ACNT electrodes. Finally, oxygenated functionalization of the ACNTs by plasma etching introduces additional pseudocapacitance to the ACNT electrode. Capacitance of a carbon-based electrode consists of two major components [2], i.e., the electri-

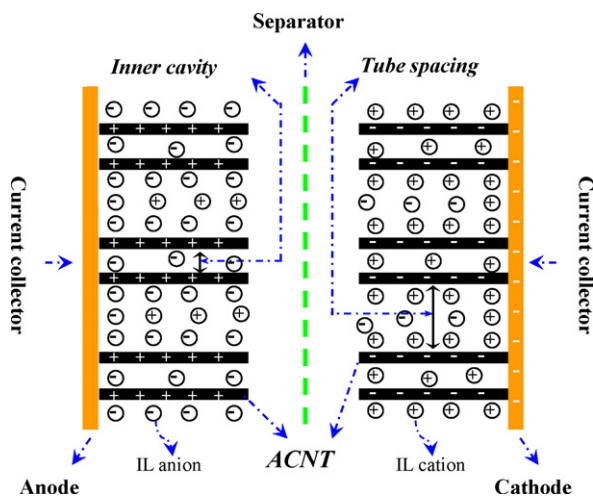


Fig. 3. Schematic of an electrochemical capacitor based on plasma-etched ACNT electrodes and ionic liquid electrolyte. Each of the constituent aligned tubes is connected directly onto a common current collector, maximizing charge transport capability of the ACNT electrode. This ensures a combined charge capacity from all individual tubes and thus an enhanced energy density for the capacitor. In turn, the stored charge can be delivered rapidly through each individual tube of the electrode, resulting in a high power density for the capacitor.

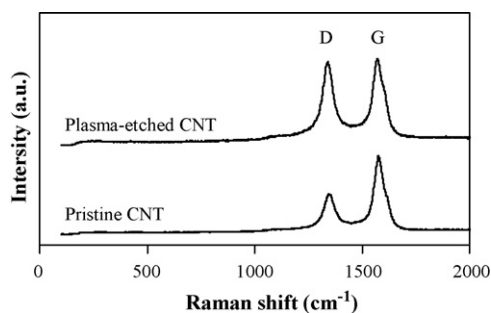


Fig. 4. Raman spectra of an ACNT electrode before and after plasma etching.

cal double-layer capacitance due to the electrostatic attraction of charged carbon surfaces to electrolyte ions and the pseudocapacitance due to the Faradic reactions of electroactive species on the carbon surfaces. The latter arises from the surface functionalization of the CNTs. Usually, presence of oxygenated functional groups on the nanotubes and their Faradic reactions upon charge and discharge of the capacitor has been considered to be an important type of pseudocapacitance for carbon-based electrode materials [10,44]. Upon plasma etching, large amount of oxygen content was observed for our ACNTs (Fig. 5), indicating the formation of oxygenated functionalization groups on these nanotubes. Electrochemically, the Faradic contribution from the redox reactions of these elec-

troactive surface groups can be evidenced by the butterfly-shape CV (and hence the potential-dependent capacitance) of the ACNT electrode (Fig. 2(A)), which is different from a typical rectangle-shape CV of a pure double-layer capacitance. Similarly, a recent work attributed the butterfly-shape CV of SWCNTs to the electrochemical doping of semiconducting nanotubes and pointed out the importance of this unique mechanism in enhancing energy storage capability for CNT capacitors [45]. Importantly, the redox processes of our ACNTs are rapid and reversible, advantageously introducing additional pseudocapacitance to the ACNT electrode. As a result, combining the enhanced double-layer capacitance (due to the vertical alignment and well spacing of ACNTs and the plasma-etch-deduced end-tip-opening and defect formation) and the additional pseudocapacitance (due to the plasma-etch-deduced oxygenated functionalization), the ACNT electrode showed a remarkable capacitance (440 F g^{-1}) in the IL electrolyte [EMIM][Tf₂N]. Previously, with the combined contribution of double-layer capacitance and pseudocapacitance, a high overall capacitance has been obtained for a template-synthesized aligned CNT electrode (365 F g^{-1}) [8] and a tubes-in-tube multi-walled CNT electrode (315 F g^{-1}) [46], in an aqueous H₂SO₄ electrolyte. The improved capacitance of the ACNT electrode observed in the present work is believed to be due to the unique properties and the advantages of plasma etching of the ACNTs as discussed above. Importantly, in conjunction with the large electrochemical windows of ILs, this would be able to significantly boost the energy density for the ACNT-IL electrochemical capacitors.

Also shown in Fig. 2(A), upon the increase in potential scan rates, the ACNT electrode still showed sharp transient responses at both ends of the CV and maintained a high capacitance. The capacitance retained 75% when the scan rate increased from 5 to 100 mV s^{-1} . This suggests a high rate capability of the ACNT electrode in the IL electrolyte. It is known that the relatively high viscosity of ILs comparing to conventional aqueous and organic electrolytes is disadvantageous for electrochemical applications (with traditional electrode materials). Our observation here indicates that, with their unique properties, the plasma-etched ACNTs are appropriate electrode materials to overcome this problem, showing highly capacitive behavior even in an IL.

Under the same conditions, a high-surface-area AC electrode [3] showed a much smaller capacitance of about 90 F g^{-1} (at 1 V) (Fig. 2(B)). Increasing the scan rate from 5 to 100 mV s^{-1} , this capacitance decreased sharply to 32 F g^{-1} (capacitance retention: 33%), accompanying with the disappearance of the rectangle-shape of the CV. This indicates the slower charge/discharge kinetics of ACs in the IL electrolyte and clearly suggests that, in order to explore the large electrochemical windows of ILs to improve performance for electrochemical capacitors (Eqs. (1) and (2)), plasma-etched ACNTs (rather than traditional ACs) are appropriate electrode materials.

Subsequently, the promising results of the plasma-etched ACNT electrodes with the [EMIM][Tf₂N] electrolyte prompted construc-

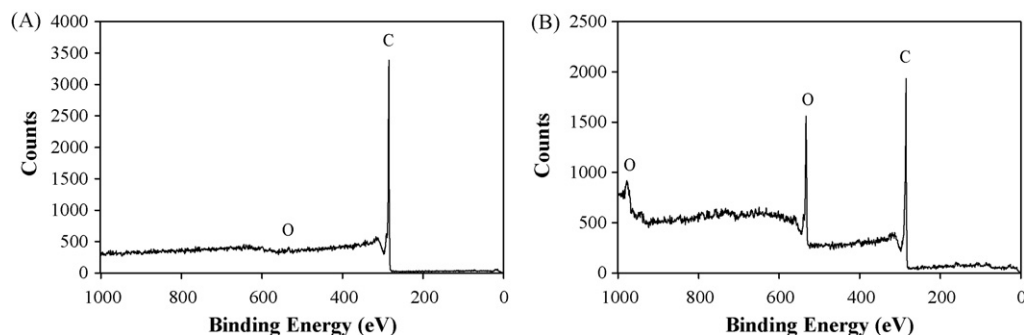


Fig. 5. XPS spectra of an ACNT electrode before (A) and after (B) plasma etching.

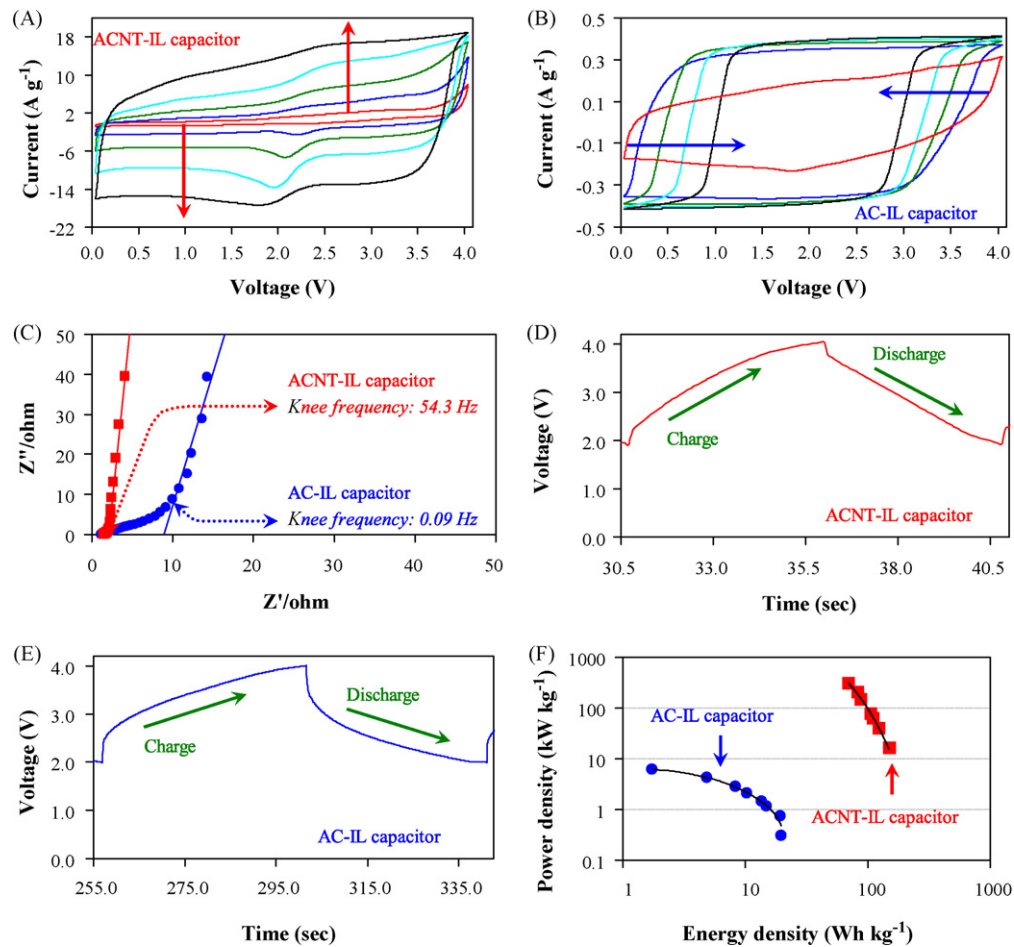


Fig. 6. Electrochemical and capacitive behavior of electrochemical capacitors fabricated from [EMIM][Tf₂N] and different electrode materials. (A and B): CVs obtained for an ACNT-IL capacitor (A) and an AC-IL capacitor (B) at the scan rate increasing from 5, 20, 50, 100, to 200 mV s⁻¹ as indicated by arrows. (C) AC impedance spectra of the capacitors (recorded at open-circuit). AC voltage amplitude: 5 mV. Frequency range: 100 kHz to 1 MHz. (D and E): Galvanostatic charge/discharge curves of the ACNT-IL capacitor (D) and the AC-IL capacitor (E). Current density: 10 mA cm⁻². Cut-off voltage: 2.0/4.0 V. (F) Ragone plots of the capacitors. Galvanostatic charge/discharge current density: 2–50 mA cm⁻². Cut-off voltage: 2.0/4.0 V. Performances of the capacitors are based on the mass of ACNT or AC of the electrode materials.

tion of prototype electrochemical capacitors (*i.e.*, ACNT-IL capacitor, Fig. 3). AC electrodes were also used to fabricate an AC-IL capacitor for reference. Due to the large electrochemical window of [EMIM][Tf₂N], both capacitors showed a high cell voltage of 4 V. However, at the scan rate greater than 20 mV s⁻¹, the AC-IL capacitor showed a fairly unchanged current and a “shrunk” CV (shown by arrows in Fig. 6(B)) due to the poor capacitive behavior (especially limited rate capability) of ACs in the IL. In contrast, the superior charge storage and delivery capability of the ACNT-IL capacitor can be seen by its continuously increasing current whilst retaining the rectangular CV, even at scan rates up to, but not limited by, 200 mV s⁻¹ (Fig. 6(A)). Moreover, the ACNT-IL capacitor showed an additional redox process at around 2 V in the CV. As discussed for Fig. 2(A), this is likely due to the pseudocapacitance contribution from the surface oxygenated functionalization of the ACNT electrodes. The significance is that the additional redox processes deduced from these electroactive species are fast and reversible, advantageously introducing additional Faradic charge storage to the capacitor. Combining with the double-layer capacitance, this significantly enhances the energy storage capability for the ACNT capacitor.

Superior capacitive behavior of the ACNT-IL capacitor has also been confirmed using AC impedance analysis (Fig. 6(C)). The results show a negligible 45° Warburg region (indicating fast ion transport at the electrode–electrolyte interface), a steep low-frequency line,

and a very high knee frequency of 54.3 Hz (indicating the ability for the capacitor to react to fast charging and discharging events). In contrast, the AC-IL capacitor displayed an expanded 45° Warburg region (indicating slow ion transport), a less steep low-frequency line, and a small knee frequency of 0.09 Hz. The knee frequency of the ACNT-IL capacitor is much higher than the usual <1 Hz of most commercially available electrochemical capacitors, including those specifically designed for high power applications [47]. This suggests that most of the stored energy in the ACNT-IL capacitor is accessible even at frequencies up to and above 50 Hz, very useful for high demand applications such as hybrid electrical vehicles (HEVs). This also indicates that the vertically aligned and unbundled structures of the plasma-etched ACNTs significantly overcome the previously perceived disadvantage of high viscosity of the IL by providing a highly accessible pathway to the IL ions (Fig. 3).

Upon galvanostatic charging/discharging, a slow discharge process was observed for the AC-IL capacitor as evidenced by a large IR drop and the bent discharge curve (Fig. 6(E)). Again, this is attributable to the high interfacial resistance and slow ion transport at the interface between the AC electrode and the IL electrolyte. In contrast, the ACNT-IL capacitor can be charged/discharged rapidly, showing a small IR drop and the well-defined discharge straight line (Fig. 6(D)). From the discharge curves obtained at a range of current densities, energy and power densities of both capacitors were calculated and presented in Ragone plots (Fig. 6(F)).

As can be seen, the AC-IL capacitor showed a much smaller performance than the ACNT-IL capacitor. Also, the increase in power density of the AC-IL capacitor was accompanied by a sharp decrease in energy density, indicating that the stored energy could not be delivered in a fast manner. Based on a simplified estimation method [48], the maximum energy density (19.6 Wh kg^{-1}) and power density (6.3 kW kg^{-1}) of the AC-IL capacitor can be translated to 6.9 Wh kg^{-1} and 2.2 kW kg^{-1} for a packaged capacitor, slightly exceeding those of the current electrochemical capacitor technology [3]. This improvement can be attributed to the high cell voltage of the AC-IL capacitor, *i.e.*, 4 V versus that (about 2.5 V) of commercially available electrochemical capacitors. However, this also indicates that, to more efficiently utilize the large electrochemical window of the IL to improve the performance for electrochemical capacitors, a specially-designed electrode material is needed. Indeed, using plasma-etched ACNT electrodes in the present work, the resultant ACNT-IL capacitor can store much more energy and in-turn deliver this energy rapidly to achieve a higher power. As illustrated in Fig. 3, each of the constituent aligned tubes of the ACNTs is connected directly onto a common current collector, maximizing charge transport capability of the ACNT electrode. This allows the rapid delivery of capacitor's stored charge through each individual tube of the electrode, ensuring a superior power density for the capacitor. A high energy density of up to 100 Wh kg^{-1} has been maintained even when a power density of as high as 100 kW kg^{-1} was reached. Further, the maximum energy density (148 Wh kg^{-1}) and power density (315 kW kg^{-1}) of the ACNT-IL capacitor are greater than those reported for CNT electrochemical capacitors fabricated from aqueous electrolytes [6,9,12]. It is the combination of the unique properties of plasma-etched ACNTs with the large electrochemical window of ILs in the present cell design that is responsible for this achievement. Using the simplified estimation method [48], the maximum energy density and power density of the ACNT-IL capacitor can be translated to 52 Wh kg^{-1} and 110 kW kg^{-1} for a packaged capacitor, significantly exceeding those of the current electrochemical capacitor technology [3]. Moreover, to make these capacitors practically useful, our future work will investigate approaches to increase the CNT loading of the ACNT electrodes to enhance volumetric performance of the capacitors. This, for example, can be fulfilled by increasing the length (*e.g.*, super-long CNTs) [49] and/or packing density (*e.g.*, highly densely packed CNTs) [14] of the CNTs. Finally, in view of the excellent safety-related properties of ILs, the environmental stability of CNTs, as well as the achievements demonstrated for other electrochemical systems incorporating ILs [20], superior safety and lifetimes can be expected for the ACNT-IL electrochemical capacitors.

4. Conclusions

With the unique properties of vertically aligned and plasma-etched carbon nanotubes, we have obtained high charge storage/delivery capability for carbon nanotube electrodes in ionic liquid electrolytes. Combining these new electrode and new electrolyte materials, we have developed new electrochemical capacitors with high cell voltages (4 V), high energy density (148 Wh kg^{-1}), and high power density (315 kW kg^{-1}), potentially exceeding those of the current electrochemical capacitor technology. The energy density demonstrated with these electrochemical capacitors is approaching the high energy realm of batteries. Inherent high rate capability of aligned carbon nanotubes provides a high power density for these capacitors. Achieving both high energy and high power densities for a same energy storage device has attracted considerable attention in energy storage community [50,51]. The device design incorporating aligned nanostructured electrodes and ionic liquid electrolytes developed in this work would benefit the high energy/high power energy storage technologies. Moreover, supe-

rior safety-related properties of ionic liquid electrolytes would ensure excellent safety and lifetimes for these new energy storage technologies.

Acknowledgements

This material is based upon work supported by the US National Science Foundation under the SBIR program (grant numbers: OII-0610919 and IIP-0724468). The authors gratefully acknowledge W.L. Gore & Associates, Inc. for providing activated carbon electrodes and poly(tetrafluoroethylene) (PTFE) membranes and Air Force Office of Scientific Research for partial financial support.

References

- [1] A. Burke, *J. Power Sources* 91 (2000) 37.
- [2] B.E. Conway, In *Electrochemical Supercapacitors: Scientific Fundamentals and Technological Applications*, Kluwer Academic/Plenum Publishers, New York, 1999.
- [3] A. Burke, M. Arulepp, *Electrochem. Soc. Proc. PV 2001-21* (2001) 576.
- [4] E. Frackowiak, F. Béguin, *Carbon* 39 (2001) 937.
- [5] S. Iijima, *Nature* 354 (1991) 56.
- [6] C. Niu, E.K. Sichel, R. Hoch, D. Moy, H. Tennent, *Appl. Phys. Lett.* 70 (1997) 1480.
- [7] R.H. Baughman, A.A. Zakhidov, W.A. de Heer, *Science* 297 (2002) 787.
- [8] Q.L. Chen, K.H. Xue, W. Shen, F.F. Tao, S.Y. Yin, W. Xu, *Electrochim. Acta* 49 (2004) 4157.
- [9] K.H. An, W.S. Kim, Y.S. Park, J.-M. Moon, D.J. Bae, S.C. Lim, Y.S. Lee, Y.H. Lee, *Adv. Funct. Mater.* 11 (2001) 387.
- [10] E. Frackowiak, K. Metenier, V. Bertagna, F. Béguin, *Appl. Phys. Lett.* 77 (2000) 2421.
- [11] A.B. Dalton, S. Collins, E. Muñoz, J.M. Razal, V.H. Ebron, J.P. Ferraris, J.N. Coleman, B.G. Kim, R.H. Baughman, *Nature* 423 (2003) 703.
- [12] S. Talapatra, S. Kar, S.K. Pal, R. Vajtai, L. Ci, P. Victor, M.M. Shaijumon, S. Kaur, O. Nalamasu, P.M. Ajayan, *Nature Nanotechnol.* 1 (2006) 112.
- [13] Ch. Emmenegger, Ph. Mauron, P. Sudan, P. Wenger, V. Hermann, R. Gallay, A. Züttel, *J. Power Sources* 124 (2003) 321.
- [14] D.N. Futaba, K. Hat, T. Yamada, T. Hiraoka, Y. Hayamizu, Y. Kakudate, O. Tanaike, H. Hatori, M. Yumura, S. Iijima, *Nat. Mater.* 5 (2006) 987.
- [15] Y. Honda, T. Haramoto, M. Takeshige, H. Shiozaki, T. Kitamura, M. Ishikawa, *Electrochem. Solid-State Lett.* 10 (2007) A106.
- [16] T.Q. Duong, 2003 Annual Progress Report for Energy Storage Research and Development (FreedomCAR & Vehicle Technologies Program, Energy Storage Research & Development, U.S. Department of Energy, May 2004).
- [17] J.P. Zheng, J. Huang, T.R. Jow, *J. Electrochem. Soc.* 144 (1997) 2026.
- [18] K. Xu, *Chem. Rev.* 104 (2004) 4303.
- [19] P. Walden, *Bull. Acad. Imper. Sci. (St. Petersburg)* (1914) 1800.
- [20] W. Lu, A.G. Fadeev, B. Qi, E. Smela, B.R. Mattes, J. Ding, G.M. Spinks, J. Mazurkiewicz, D. Zhou, G.G. Wallace, D.R. MacFarlane, S.A. Forsyth, M. Forsyth, *Science* 297 (2002) 983.
- [21] T. Fukushima, A. Kosaka, Y. Ishimura, T. Yamamoto, T. Takigawa, N. Ishii, T. Aida, *Science* 300 (2003) 2072.
- [22] R.D. Rogers, K.R. Seddon, *Science* 302 (2003) 792.
- [23] M.C. Buzzeo, R.G. Evans, R.G. Compton, *Chem. Phys. Chem.* 5 (2004) 1106.
- [24] J.N. Barisci, G.G. Wallace, D.R. MacFarlane, R.H. Baughman, *Electrochem. Commun.* 6 (2004) 22.
- [25] B. Xu, F. Wu, R. Chen, G. Cao, S. Chen, G. Wang, Y. Yang, *J. Power Sources* 158 (2006) 773.
- [26] H. Zhang, G. Cao, Y. Yang, *Nanotechnology* 18 (2007) 195607.
- [27] H. Zhang, G. Cao, Y. Yang, Z. Gu, *J. Electrochem. Soc.* 155 (2008) K19.
- [28] S. Huang, L. Dai, A.W.H. Mau, *J. Phys. Chem. B* 103 (1999) 4223.
- [29] S. Huang, L. Dai, *J. Phys. Chem. B* 106 (2002) 3543.
- [30] J. Yang, L. Dai, R.A. Vaia, *J. Phys. Chem. B* 107 (2003) 12387.
- [31] W.-C. Fang, *J. Phys. Chem. C* 112 (2008) 11552.
- [32] W. Lu, K. Henry, C. Turchi, J. Pellegrino, *J. Electrochem. Chem.* 155 (2008) A361.
- [33] M. Galiński, A. Lewandowski, I. Stępnik, *Electrochim. Acta* 51 (2006) 5567.
- [34] A. Peigney, Ch. Laurent, E. Flahaut, R.R. Bacsa, A. Rousset, *Carbon* 39 (2001) 507.
- [35] E. Frackowiak, F. Béguin, *Carbon* 40 (2002) 1775.
- [36] D. Zilli, P.R. Bonelli, A.L. Cukierman, *Nanotechnology* 17 (2006) 5136.
- [37] Z. Yang, H. Wu, *Solid State Ionics* 143 (2001) 173.
- [38] N.S. Kim, J. Park, J.H. Ryu, H.J. Lee, S.Y. Choi, J. Choo, *J. Phys. Chem. B* 106 (2002) 9286.
- [39] J.J. Gooding, *Electrochim. Acta* 50 (2005) 3049.
- [40] G.G. Wildgoose, C.E. Banks, R.G. Compton, *Small* 2 (2006) 182.
- [41] C.E. Banks, T.J. Davies, G.G. Wildgoose, R.G. Compton, *Chem. Commun.* 7 (2005) 829.
- [42] K. Gong, Y. Yan, M. Zhang, L. Su, S. Xiong, L. Mao, *Anal. Sci.* 21 (2005) 1383.
- [43] S. Chakrabarti, K. Gong, L. Dai, *J. Phys. Chem. C* 112 (2008) 8136.
- [44] Y.T. Kim, Y. Ito, K. Tada, T. Mitani, U.-S. Kim, H.S. Kim, B.W. Cho, *Appl. Phys. Lett.* 87 (2005) 234106.
- [45] O. Kimizuka, O. Tanaike, J. Yamashita, T. Hiraoka, D.N. Futaba, K. Hata, K. Machida, S. Suematsu, K. Tamamitsu, S. Saeki, Y. Yamada, H. Hatori, *Carbon* 46 (2008) 1999.

- [46] H. Pan, C.K. Poh, Y.P. Feng, J. Lin, *Chem. Mater.* 19 (2007) 6120.
- [47] J.R. Miller, in: F. Delnick, M. Tomkiewicz (Eds.), *ECS Symposium Proceedings, The Electrochemical Society* 1996, p. 246.
- [48] M. Mastragostino, C. Arbizzani, R. Paraventi, A. Zanelli, *J. Electrochem. Soc.* 147 (2000) 407.
- [49] K. Hata, D.N. Futaba, K. Mizuno, T. Namai, M. Yumura, S. Iijima, *Science* 306 (2004) 1362.
- [50] P.L. Taberna, S. Mitra, P. Poizot, P. Simon, J.-M. Tarascon, *Nat. Mater.* 5 (2006) 567.
- [51] K. Kang, Y.S. Meng, J. Bréger, C.P. Grey, G. Ceder, *Science* 311 (2006) 977.